Peroxyacetyl nitrate (PAN) in the border of Beijing, Tianjin and Hebei of China: Concentration, source apportionment and photochemical pollution assessment

Wei Wei, Jiaxin Zang, Xiaoqi Wang, Shuiyuan Cheng

PII: S0169-8095(20)30054-5

DOI: https://doi.org/10.1016/j.atmosres.2020.105106

Reference: ATMOS 105106

To appear in: *Atmospheric Research*

Received date: 12 January 2020

Revised date: 30 April 2020

Accepted date: 10 June 2020

Please cite this article as: W. Wei, J. Zang, X. Wang, et al., Peroxyacetyl nitrate (PAN) in the border of Beijing, Tianjin and Hebei of China: Concentration, source apportionment and photochemical pollution assessment, *Atmospheric Research* (2019), https://doi.org/10.1016/j.atmosres.2020.105106

Peroxyacetyl nitrate (PAN) in the border of Beijing, Tianjin and Hebei of China: concentration, source apportionment and photochemical pollution assessment

Wei Wei[a,b*], Jiaxin Zang[a], Xiaoqi Wang[a], Shuiyuan Cheng[a,b]

a Department of Environmental Science and Engineering, Beijing University of Technology, Beijing, 100124, China
b Key Laboratory of Beijing on Regional Air Pollution Control, Beijing, 100124, China

Abstract

A one-year observation of atmospheric peroxyacetyl nitrate (PAN) in the border of Beijing-Tianjin-Hebei (BTH) was conducted during 2018~2019 to assess the photochemical pollution in this region. PAN daily average was 2.23, 3.72, 5.34 and 2.44 ppb(v) in October, January, April and July. The higher PAN here compared to previous studies on urban Beijing implies the deterioration of photochemical pollution in BTH region. High positive correlation between PAN and CO in October and January points to the important role of tropospheric accumulation in PAN level in fall and winter; while $\Delta O_3/\Delta PAN$ analysis implies that the photochemical pollution was more aged in this border than in urban Beijing, and more aged in October than in April. Based on the calculations of PAN photochemical formation and thermal decomposition, PAN yield rate was determined, 0.20, 0.07, 0.47 and 0.08 ppt·s^{-1} for daily average, 0.87, 0.32, 0.95 and 0.93 ppt·s^{-1} for daily maximum, respectively in October, January, April, and July. Local photochemical pollutions still existed in the border of BTH in non-winter seasons. Potential source contribution function analysis (PSCF) found that the grids that most potentially contribute to high PAN appeared around the border site in July, 50~100 km away in direction of southwest in January, both around this site and along the southern trajectory clusters in October and April. Transport of PAN from South Hebei and Tianjin to Beijing could be seen in non-summer seasons. Regression analyses further quantified the contribution of regional transport to PAN in the border, roughly 65% (April and October), 93%

* corresponding author: weiwei@bjut.edu.cn

(January) and 48% (July) at noon time. Finally, the comparison in PAN during 12:00-16:00 under various winds explores the more severe photochemical pollutions in South Hebei and Tianjin compared to Beijing in non-summer seasons, but the same level of photochemical pollutions in various cities of BTH in summer.

Keywords: PAN; photochemical pollution; source apportionment; North China

1. Introduction

Associated with the serious aerosol pollution, photochemical smog and precipitation acidification, nitrogen oxides (NO_x) and their oxidization products (NO_z) play a significant role in the chemistry of urban polluted atmosphere (Russell et al., 1985; Bytnerowicz and Fenn, 1996; Ma et al., 2018). A major question in the atmospheric nitrogen chemistry is the identity and the distribution between the ultimate products in the atmosphere. Peroxyacetyl nitrate (PAN), as an important constitute of nitrogen chemistry and the reservoir for reactive nitrogen in the condition of low temperature, is necessarily been taken into account, including its transport behavior and chemical process (Singh and Salas, 1983; Fischer et al., 2010; Hudman et al., 2004; So and Wang, 2003; Zeng et al., 2019). Moreover, PAN originates only from atmospheric photochemical reactions and has very short lifetime to decomposed completely in high temperature (30 min under 298K and 10 days under 273K), so the here presence of PAN could indicate the occurrence of photochemical pollution and is always considered as a fair indicator of photochemical pollution (Fischer et al., 2014; McFadyen and Cape, 2005).

On the other hand, China is believed to be highly photochemical polluted, particularly the North China (Cooper et al., 2014; Dufour et al., 2018). Based on ground ozone (O_3) observations, photochemical pollution (daily maximum 8-hour O_3 exceeding 160 $\mu g \cdot m^{-3}$) frequently occurs during May to Sep in North China. The data published by China's national air quality monitoring system (www.mep.gov.cn), revealed a continuous increasing in daily maximum 8-hour O_3 of May-Sep in major cities of North China during 2014~2018, rising roughly from 124.7 $\mu g \cdot m^{-3}$ to 142.8 $\mu g \cdot m^{-3}$ in Bohai Rim area, from 118.8 $\mu g \cdot m^{-3}$ to 154.2 $\mu g \cdot m^{-3}$ in southern Hebei, from

106.0 μg·m^{-3} to 127.8 μg·m^{-3} in northern Hebei, from 118.6 μg·m^{-3} to 150.8 μg·m^{-3} in Shandong (Chen et al., 2019). Li et al. (2019) also found an annual increase of 3.1 ppb(v) in O_3 during 2013~2017 in Beijing-Tianjin-Hebei region (BTH). The photochemical pollution status and its source apportionment in this region becomes an important issue. Compared to O_3, PAN is less influenced by long-range transport for its short lifetime during non-winter seasons and more accurately represents the local photochemical pollution problem. And PAN combining with O_3 would be more helpful to understand the chemistry nature of photochemical pollution.

A large number of observation studies on PAN were conducted in North China, but most of them gave attention to the hot season and the urban area, as shown in Table 1. These previous studies obtained the mean value of daily PAN of 0.97~3.98 ppb(v) in hot season and 0.28~2.10 ppb(v) in cold season, generally higher than that in developed regions (Malley et al., 2016; Pandey Deolal et al., 2014). Diurnal PAN was measured to have the high level during daytime and low level during nighttime, with the peak at 14:00-16:00 of local time, for PAN formation exclusively depends on hydroxyl radicals (OH) that is produced from photolysis. But, seasonal variation of PAN is still speculative. Zhang et al. (2014a) observed the trend of summer>winter in urban Beijing, while divergent trends were measured in other urban or suburban areas (Beine and Krognes, 2000; Lee et al., 2013; Wang et al., 2015). The correlation analysis in previous studies found that PAN positively responded to O_3 in summer but not in winter in urban Beijing (Liu et al., 2018; Qiu et al., 2019; Zhang et al., 2014b). It seems to imply that Beijing PAN was mostly contributed by photochemical reactions in summer, but dominantly determined by the accumulation and transport in winter for the longer lifetime of PAN in low temperature. While the high positive-correlation between PAN and NO_2 in winter of urban Beijing obtained by Zhang et al. (2014b) seems to indicate the significant influence of precursor on PAN through photochemical reactions in winter. Overall, regarding PAN, there is still a gap to be well understood for its pollution status, chemistry formation process, and regional transport influence in different areas of North China.

This study focuses on the border of Beijing, Tianjin and Hebei, and tries to discuss

the photochemical pollution problem in BTH regional scale through conducting a one-year observation campaign on PAN there. Our observation site is far away from industrial manufacturing and residential settlements, and mainly reflects the influence of transport of primary precursors and photochemical aging air-masses from neighbor cities. We think that this study on PAN and its source apportionment in this border will improve our understanding of the regional photochemical pollution status, local chemical formation, and transport among several major cities in BTH region.

Table 1 PAN level in previous studies on North China (ppb)

Study period	Location	average	peak	Reference
Aug of 2005-2009	Beijing, urban	0.56-2.17		Gao et al., 2014
Aug 2006	Beijing, urban	1.41	11.2	Zhang et al., 2011
Sept 2006	Beijing, rural	0.6	2.5	
Aug 2007	Beijing, urban	3.79	17.8	Xu et al., 2011
Jul-Aug 2008	Beijing, suburban		9.3	Xue et al., 2014
Jan-Mar 2010	Beijing, urban	0.7	3.5	Zhang et al., 2014b
Jun-Sept 2010	Beijing, urban	2.0	12.5	Zhang et al., 2015
Oct 2010-Mar 2011	Beijing, urban	0.28-0.73		Zhang et al., 2014a
Mar- Aug 2011	Beijing, urban	1.37-3.79		
Aug of 2006-2014	Beijing, urban	0.5~3.0	6~17	Zhang et al., 2017
Jun-Jul 2014	Baoding, rural	0.7~3.1		
Dec 2015-Mar 2016	Beijing, rural	1.04	5.96	Zhang et al., 2019
Nov 2015-Jan 2016	Jinan, urban	1.9	9.6	Liu et al., 2018
Apr-Jul 2016	Jinan, urban	2.5	13.5	

2 Experimental procedures

2.1 geographical and meteorological conditions of the border site

Our observation site (TS, 116.79° E, 39.62° N) is located in the border zone of Beijing city, Tianjin city and Hebei province, about 50 kilometers southeast from Beijing center, 70 kilometers northwest from Tianjin center, 13 kilometers and 140 kilometers northeast from Langfang city and Baoding city of Hebei province, as shown in **Fig.1**. No substantial industrial- and residential- activities surround this site, so its air quality is mainly determined by the transport of polluted air masses from neighbor cities. This border site could be considered as a regional transport evaluation site. Regarding PAN at this border site, local photochemical reactions partly

contribute, for massive anthropogenic precursors of PAN can be delivered here from near cities; on the other hand, PAN produced in near cities can also be transferred here with winds. So, there is a potential photochemical pollution and a possible high-level of PAN.

The PAN observation is conducted in October of 2018, January, April and July of 2019. The sampling site is at the roof of a four-story building and there is no large-scale construction around the site. The probability of surface winds during studied periods are presented in **Fig. 2**. It can be seen that northeasterly winds and southwesterly winds prevailed in this area, respectively with occurrence proportion of 34% and 16% in October, 32% and 29% in January, 21% and 40% in April, 29% and 27% in July; while, northerly and northwesterly winds frequently occurred in October (33%) and in January (26%). It means that this border site was mainly under the influences of southwesterly air masses passing over South Hebei and northeasterly air masses passing over Tangshan city of North Hebei. In addition, the influence of northerly or northwesterly air masses passing over Beijing on this site was still prominent in fall and winter.

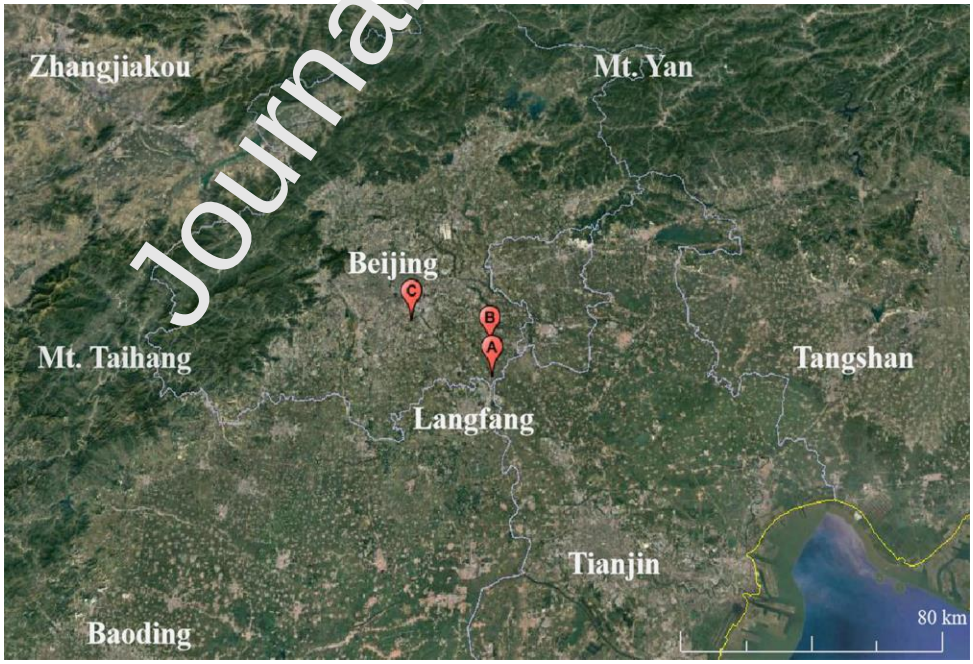

Fig. 1 Map showing the locations of PAN observation site TS (A), YLD air quality monitoring station (B), and the meteorological monitoring station (C)

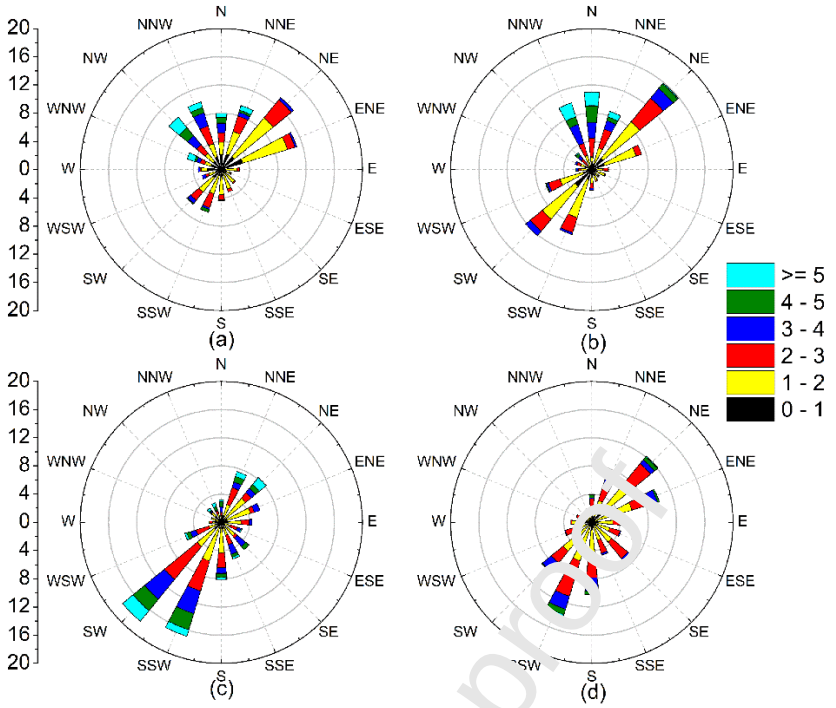

Fig. 2 Winds at 10m in Oct 2018 (a), Jan 2019 (b), Apr 2019 (c), and Jul 2019(d) at the meteorological monitoring station

2.2 Measurement of PAN in the atmosphere

We use an online PAN analyzer (Beijing Convenient Environmental Tech Co. Ltd.) to continually and automatically measure ambient PAN concentration during our studied periods. This PAN analyzer is composed of gas chromatograph (GC) and electron capture detector (ECD). Temperature of the GC oven and ECD detector was maintained at 5°C and 39°C respectively. The ambient air sample was firstly drawn through a Teflon tube to a loop (1 cm^3) by a micro vacuum pump with a flow rate of 18 mL min^{-1}, and then was delivered to the GC by the carrier gas of He. The detection limit was values about 20 ppt(v) and the time resolution was 10 min.

For the way of calibrating PAN, under the irradiating of UV lights (λ=285 nm), a large amount of acetone was firstly photolyzed to form sufficient peroxyacetyl radicals, and then reacted with the quantified NO to produce PAN with a precise concentration. We used 5 concentration levels (1.28, 3.84, 6.36, 8.90, 11.40 ppb) to make the calibration lines, and finished one calibration line each week. The R^2 of calibration lines could reach >0.96, and overwhelmingly >0.99.

2.3 Data for meteorological parameters and air pollutants

Atmospheric pollutants of NO_2, O_3, CO and $PM_{2.5}$ were the concern of this study, in order to explore the photochemical formation of PAN. We chose YLD air quality monitoring station (116.78° E, 39.71° N, **Fig. 1**) and collected the hourly concentrations of these pollutants through China's national air quality monitoring system (www.mep.gov.cn). YLD station is the nearest air quality station to our PNA observation site, and the distance between them is ~10 km.

Surface meteorological data were from the Chinese national meteorological monitoring system (http://data.cma.cn) at the 54511 station (116.47° E, 39.80° N, **Fig. 1**), including wind speed at 10 m (WS), wind direction at 10 m (WD), temperature at 1.5 m (T), and relative humidity at 1.5 m (RH). The meteorological station has an effective distance of ~30 km in plain area, and its meteorological data could represent the meteorological condition in the border of BTH.

2.4 Potential source contribution function (PSCF) analysis

Potential source contribution function (PSCF) analysis was conducted here to determine the most probable source regions of PAN observed at this border site. First, we used HYSPLIT model (https://ready.arl.noaa.gov/HYSPLIT_traj.php) to simulate the backward trajectories of air masses at the border site (100m AGL), based on the global data assimilation system dataset (GDAS) of the U.S. National Centers for Environment Prediction (ftp://arlftp.arlhq.noaa.gov/pub/archives). The back-trajectory path was defined at 1 h backward intervals by the latitude, longitude, and height of the point. The trajectories were calculated backward for 3 days for January, 1 day for October and April, and 6 hours for July, according to the temperature-related properties of PAN lifetime.

Then, TrajStat software was utilized to do the PSCF analysis, through combining back-trajectories with PAN observations (Wang et al., 2009). The domain of interest extended from 35°~45° north latitude and 110°~122° east longitude, divided into 0.1° × 0.1° cells, and a threshold (50th percentile) of PAN concentrations was set for the criterion value. The arbitrary weigh function Polissar et al. (1999) was introduced to

the PSCF in order to avoid the uncertainties resulting from a limited amount of available data.

3 Results and discussion

3.1 Temporal variation of PAN

The time series of the mixing ratios of ambient PAN at TS during the studied period are given in **Fig. 3**, as well as ambient NO_2, O_3 and CO monitored in air quality station YLD. In the border of BTH, PAN could be detected in nearly all samples during the whole period and showed a pronounced seasonal variation. PAN daily average and daily maximum reached 2.23 and 4.67 ppb(v) in October, 3.72 and 6.06 ppb(v) in January, 5.34 and 9.10 ppb(v) in April, 2.34 and 4.95 ppb(v) in July, as shown in **Table 2**. Highest PAN occurred in spring but not in summer, although summer has the greater solar intensity and higher OH radical that favor the photochemical formation of PAN. This can be attributed to the increased thermal decomposition for PAN due to the higher temperatures in summer. On the other hand, the unexpected high levels of PAN were observed during January, which implied a possibility of severe photochemical pollution in the regional scale in winter. The high PAN in winter was also obtained Liu et al. (2018) in Jinan and by a Lee et al. (2013) in South Korea. Comparing with previous observations in urban and rural areas of Beijing as presented in Table 1, our results in October, January and July were slightly higher, and greatly higher in April. It could be explained by the temporal-spatial variation of precursors in this region during 2004 to the present. Zhang et al., (2018) found that average NO_2 column in North China had rapidly increased from ~800×10^{13} molec·cm^{-2} in 2004 to 1792×10^{13} molec·cm^{-2} in 2011, and then decreased to 1254×10^{13} molec·cm^{-2} in 2015; the high NO_2 area happened around Beijing and Tianjin during 2005-2011, but transferred to northeast Hebei (Tangshan) and south Hebei (Baoding, Shijiazhuang, Xingtai and Handan) during 2012-2015. The higher PAN in this study compared to previous studies on Beijing, implies the temporal-spatial variation of photochemical pollution in BTH region due to the increasing NO_2 in several major cities of Hebei province.

Fig. 4 describes the average diurnal profiles of PAN, O_3 and NO_2 in four studied months, as well as their ratios to CO. CO is a relatively inert compound, and the reference to CO could weaken the accumulation role of stable meteorological regimes such as small winds and low planetary boundary layer and strengthen the atmospheric chemistry role. For PAN:CO, the single-peak diurnal pattern was apparently measured in October, January and April, and peak values occurred in 14:00-16:00. This diurnal variation looks consistent with the typical solar radiation pattern and demonstrates the dominant contribution from regional photochemical pollution rather than from long-range transport to the PAN, even in January. Comparing with O_3:CO, the peak time of PAN:CO was about 1~2 hour earlier in October and April, but simultaneous in January, which illustrates that the transport of PAN in non-winter seasons is limited and even less than O_3 for its shorter lifetime. However, in July the dual-peak diurnal pattern was observed with two peaks respectively in 12:00-13:00 and in 20:00-21:00. The evident decrease of PAN and PAN:CO during 13:00-15:00 in summer days can be accounted for the rapid increase in PAN thermal decomposition, for the higher ambient temperature. For the diurnal variability of PAN and PAN:CO, April had the larger values than other three months. Between October 2018 and April 2019, the surface temperature was very similar, but NO_2 level greatly varied. High NO_2 level in April undoubtedly deteriorated the photochemical pollutions in local or regional scales and resulted in high concentration of PAN and O_3.

Table 2 Statistics of daily average and daily maximum of PAN concentrations (ppb)

	N	PAN daily average			PAN daily maximum			max	min
		mean	median	stdev	mean	median	stdev		
2018.10	576	2.23	1.28	2.17	4.67	3.61	2.99	9.82	0.11
2019.01	648	3.72	2.56	3.53	6.06	4.66	4.43	21.67	0.17
2019.04	576	5.34	4.07	3.75	9.10	6.86	5.67	26.04	0.84
2019.07	498	2.44	2.04	1.65	4.95	4.76	1.90	10.39	0.13

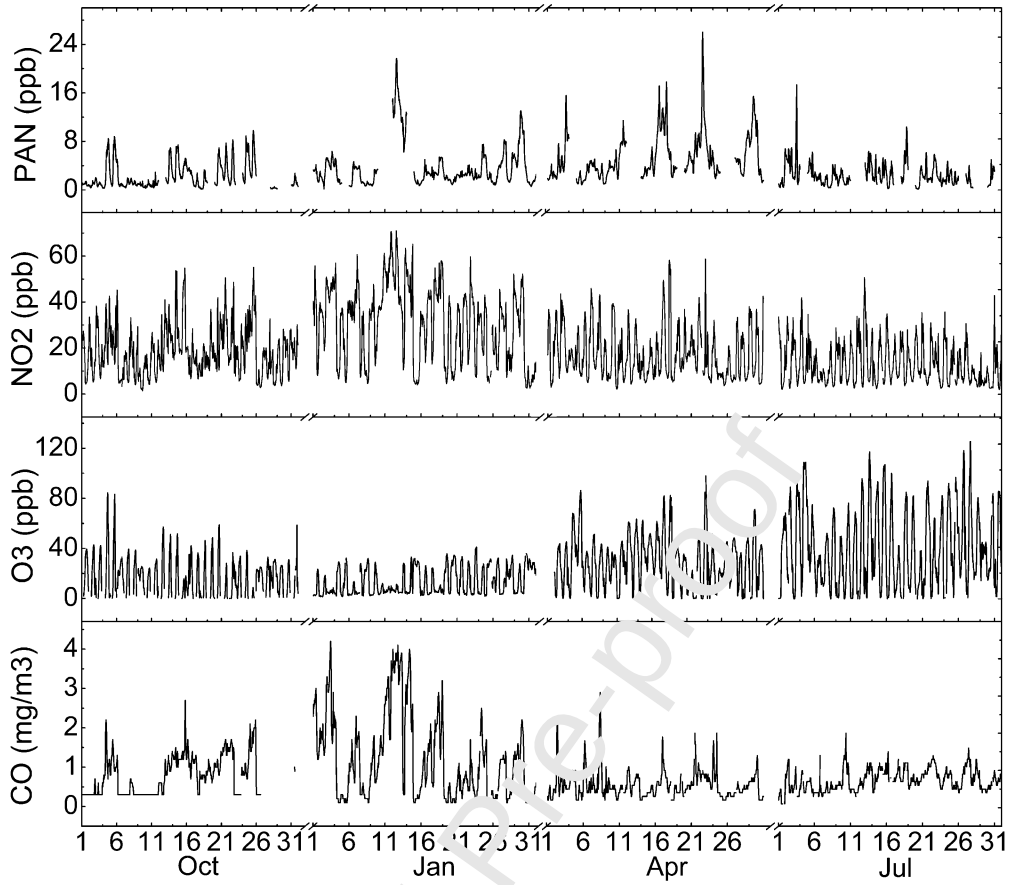

Fig. 3 time series of the mixing ratios of ambient PAN, NO_2, O_3 and CO during four studied months

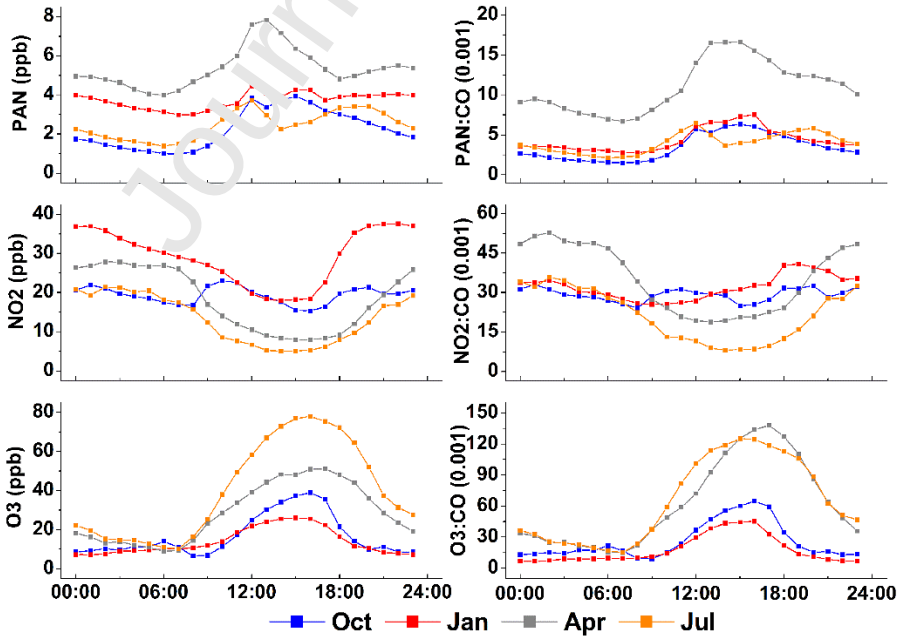

Fig. 4 Average diurnal variations of PAN, O_3, NO_2 and their ratios to CO during four studied months

3.2 Relationship with other atmospheric pollutants

Here we discuss the correlation of PAN with air pollutants of O_3, NO_2 and CO, to explore the sources of PAN in this border area. The correlation coefficient (R) reached 0.55, 0.68, 0.24 and 0.25 between hourly PAN and hourly CO, 0.55, 0.49, 0.01 and -0.02 between hourly PAN and hourly NO_2, 0.32, -0.23, 0.87 and 0.29 between daily PAN maximum and daily O_3 maximum, respectively in October 2018, January 2019, April 2019 and July 2019. The good positive correlation between PAN and CO and between PAN and NO_2 in January showed the predominant role of meteorological regimes in PAN in winter; on the contrary, their weak correlation in October, April and July implied the important influence of atmospheric chemistry on PAN in non-summer seasons.

O_3 and PAN both originate from atmospheric photochemistry, but the lifetime of O_3 is longer than that of PAN especially in non-winter days. So, the ratio of O_3 change to PAN change ($\Delta O_3/\Delta PAN$) during photochemistry enhancement time (9:00-14:00) is considered as an indicator for assessing the aging of photochemical pollution. In the same environment temperature, the higher $\Delta O_3/\Delta PAN$ value, the more aged the photochemical pollution is. In this study, the monthly $\Delta O_3/\Delta PAN$ was measured to be 18.8±8.2 in October, 10.3±6.7 in January, 9.2±4.5 in April and 23.2±10.5 in July. It implies a more aged photochemical pollution in the border of BTH in October than in April. While, comparing with ~18 value by Zhang et al. (2014a) in summer urban Beijing, the higher $\Delta O_3/\Delta PAN$ value in July of this study implies the more aged photochemical pollution in the border area than in urban Beijing.

For NOx, their correlations with PAN would be more complex. NO_2 is a key precursor of PAN photochemical formation through the reactions R1-2, and reversely responds to PAN concentration; on the other hand, abundance of NO_2 relative to NO inhibits PAN thermal decomposition through reactions R3-R4 with the temperature, and positively favors high PAN concentrations. During photochemistry enhancement time (9:00~14:00), hourly PAN:CO had a relatively moderate negative correlation with hourly NO_2 in January (R=-0.5) and a weak negative correlation in April

(R=-0.32) and July (R=-0.34), but was little correlated in October (R=-0.04). Regarding the lowest R value in October, it can be explained by the varied diurnal NO_2 level that was caused by diurnal change in winds. In October of 2018, northeastern winds prevailed in nighttime but southern and southwestern winds prevailed in daytime, as shown in **Fig. 2**. South winds moving over South Hebei and associated with more polluted air masses, so we can see a lower level of NO_2 in nighttime and a distinct increase in NO_2 from 8:00~11:00 from **Fig. 4**.

$$VOCs + \cdot OH \xrightarrow{hv} CH_3COO_2\cdot + products \quad (R1)$$

$$CH_3COO_2\cdot + NO_2 \xrightarrow{M} CH_3COO_2NO_2 \quad (R2)$$

$$CH_3COO_2NO_2 \xrightarrow{M} CH_3COO_2\cdot + NO_2 \quad (R3)$$

$$CH_3COO_2\cdot + NO \rightarrow CH_3\cdot + CO_2 + NO_2 \quad (R4)$$

3.3 PAN yield rate estimates

PAN photochemical formation deeply depends on its precursors of NO_2 and PA ($CH_3COO_2\cdot$) and can be calculated according to formula 1, where k_1 is the rate constants for Reaction R2 ($k_1=9.5\times10^{-12}$ $cm^3\cdot molecule^{-1}\cdot s^{-1}$) (Bridier et al., 1991); PAN thermal decomposition is decided by PAN level and ambient temperature and can be calculated according to formula 2, where k_2 is the rate constants for Reaction R3 ($k2=2.52\times10^{16}$ $e^{(-13533/T)}$ s^{-1}) (Tuazon et al., 1991). Thus, PAN yield rate can be determined through combining its production rate and thermal decomposition rate, as shown in formula 3. However, direct measurements of PA radical are difficult, for its very short lifetime of ~10 seconds (Lafranchi et al., 2009). In the stable atmospheric conditions, PAN variation (d[PAN]/dt) could be assumed to be decided by formation and decomposition processes but never influenced by regional transport, so PA participating in reaction R2 could be estimated according to formula 4 (Zhang et al., 2014b). Here, we further improve this method and use the PAN:CO and NO_2:CO as the substitutes for PAN and NO_2 concentrations, as presented in formula 5, to eliminate influence of physical dispersion process on PAN variation and emphasize

the role of photochemistry in PAN variation. Then, we choose 2~4 stable days (5, 14, 21 Oct; 12, 17, 18, 29 Jan; 28, 29 Apr and 9, 20, 24 Jun) when wind speed generally lower than 2 m/s and relative humidity generally higher than 60% for each month, and calculate hourly PA level for these stable days, as presented in **Fig. 5**. It can be seen that PA estimated is higher during daytime and lower during nighttime, and has highest level in July (8.80×10^{-1} ppt) than in April (3.37×10^{-1} ppt), October (1.05×10^{-1} ppt) and January (1.78×10^{-2} ppt), which is consistent with our understanding that PA radical originates mainly from photochemical reactions and previous researches. PA is difficult to be accumulated in atmosphere due to the very short lifetime, so PA concentration depends largely on time and location rather than on physical diffusion process. Here, we assumed PA in steady-state in one month, and used the estimated PA in the stable days to represent PA level of all days of the studied month. However, it needs to be noted that there will exist the small difference in PA among different days in one month, thus we calculated the PAN yield rates only for the monthly average, but not for individual days.

$$d[PAN]/dt_{\_formation} = k_1[PA][NO_2] \quad (1)$$

$$d[PAN]/dt_{\_decomposition} = k_2[PAN] \quad (2)$$

$$d[PAN]/dt = d[PAN]/dt_{\_formation} - d[PAN]/dt_{\_decomposition} \quad (3)$$

$$[PA] = (d[PAN]/dt + k_2[PAN])/k_1[NO_2] \quad (4)$$

$$[PA] = (d[PAN/CO]/dt + k_2[PAN/CO])/k_1[NO_2/CO] \quad (5)$$

Fig. 5 also gives the diurnal variations of PAN formation rate, thermal decomposition rate and yield rate on monthly average. Generally, July had the highest photochemical formation rate with the daily average of 1.88 $ppt\cdot s^{-1}$, followed by April (0.96 $ppt\cdot s^{-1}$) and October (0.48 $ppt\cdot s^{-1}$), and January had the lowest formation rate (0.091 $ppt\cdot s^{-1}$). On the other hand, thermal decomposition rate was still highest in July (1.80 $ppt\cdot s^{-1}$) than in April (0.49 $ppt\cdot s^{-1}$), October (0.28 $ppt\cdot s^{-1}$) and January (0.030 $ppt\cdot s^{-1}$). Thus, the higher PAN yield rate happened in April and October rather than in July and January. During daytime (from 9:00 to 18:00) the PAN yield rate was

positive in all months, as follows of April (0.81 ppt·s^{-1}) > October (0.50 ppt·s^{-1}) > January (0.15 ppt·s^{-1}) and July (0.11 ppt·s^{-1}); while during nighttime (from 20:00 to 6:00) PAN yield rate was positive in April (0.11 ppt·s^{-1}), but very small or even negative in July (0.007 ppt·s^{-1}), January (0.003 ppt·s^{-1}) and October (-0.026 ppt·s^{-1}).

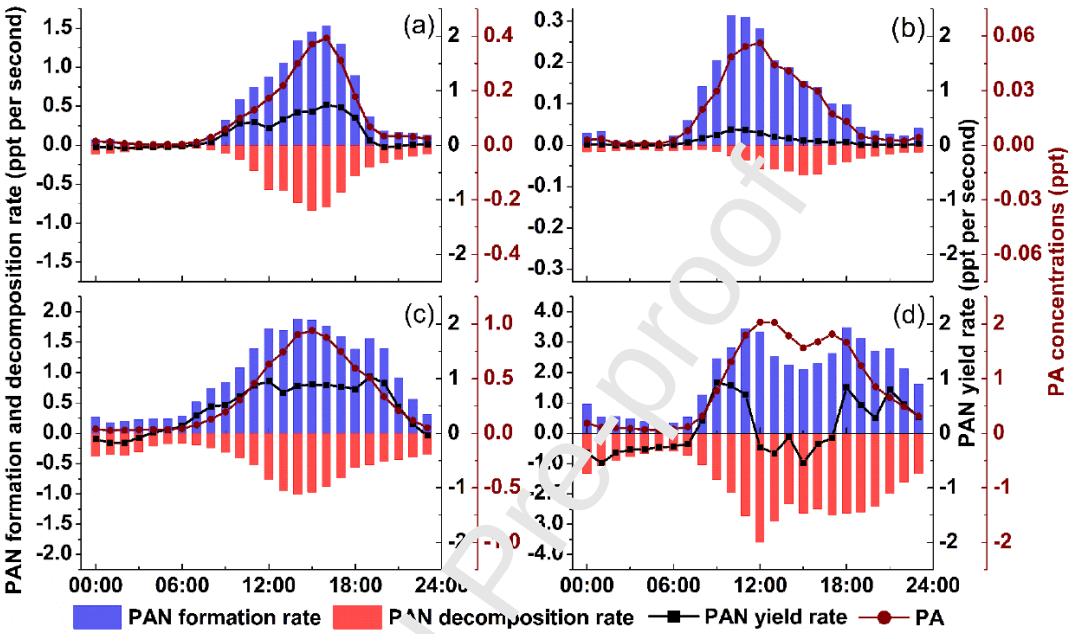

Fig. 5 The estimates of PA (red line), PAN photochemical formation rate (blue bar), thermal decomposition rate (red bar) and yield rate (black line) during Oct (a), Jan (b), Apr (c) and Jul (d)

3.4 Source apportionment on PAN

(1) PSCF analyses for four months

PSCF analyses results for four studied months are presented in **Fig. 6**, which interpret the potential contributions of the grid cells to high PAN at this border site. It can be seen that in July, the highest PSCF values gathered around the observation site in the direction of south. It indicates the predominant contribution of local photochemical pollution to PAN in this border. While, in October and April, higher PSCF values appeared both around this site in the direction of south and along the southwestern- or southern trajectory clusters, which implying physical transport from the south of Hebei was just as important to PAN of this site as local photochemical reactions. However, the transport distance was longer in April than in October, high

PSCF values covering only Langfang and southwest of Tianjin in October, but involving in Langfang, Baoding and Hengshui three cities of Hebei province in April. In January, the geographical distribution of PSCF analysis in **Fig. 6 (b)** shows higher contribution of Langfang city, northeast of Baoding city and west of Cangzhou city to PAN at our observation site. The highest PSCF values never happened around this site, but in the grids about 50~100 km southwest from our observation site, which implies the more significant contribution of regional transport to PAN compared to local photochemical reactions in winter.

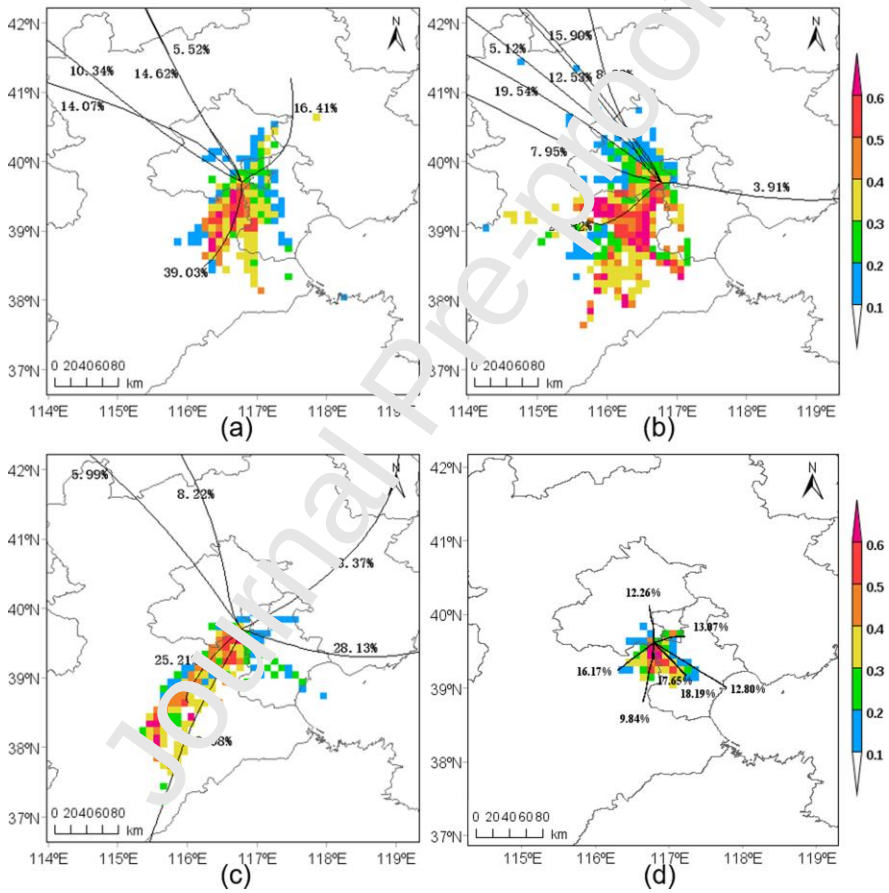

Fig. 6 PSCF (potential source contribution function) analysis values for PAN (colored block) and trajectory clustering results (black line) in Oct for 24h (a), Jan for 72h (b), Apr for 24h (c), Jul for 6h (d)

(2) Regression analyses for October and April

In order to apportion PAN measured at this site between photochemical reactions and regional transports, the statistical analyses were performed through developing the regression between PAN concentration and two variables of PAN yield rate and wind speed. The series of hourly PAN concentrations, yield rates and wind speeds

applied linear (no transformation) regression, as shown in formula 6, where β_1 represents PAN accumulation produced by local photochemical chemistry (s), β_2 represents PAN increment caused by winds transport (ppb·s·m^{-1}). Thus, the contribution of local photochemistry and regional transport to PAN can be estimated according to formula 7 and formula 8, in respective.

$$[PAN] = \beta_1 \times [PAN\ yield\ rate] + \beta_2 \times [wind\ speed] \quad (6)$$

$$\%photochemistry = \frac{\beta_1 \times [PAN\ yield\ rate]}{\beta_1 \times [PAN\ yield\ rate] + \beta_2 \times [wind\ speed]} \quad (7)$$

$$\%transport = \frac{\beta_2 \times [wind\ speed]}{\beta_1 \times [PAN\ yield\ rate] + \beta_2 \times [wind\ speed]} \quad (8)$$

Regression obtained the better performance for October 2018 (R^2 of 0.44) and April 2019 (R^2 of 0.71). Regression coefficients were calculated to be 1326 (October) and 855 (April) for β_1; 0.69 (October) and 1.78 (April) for β_2. In Beijing, the annual emission rate of SO_2 reached about 150 ton·d^{-1} recently, approximately going to 1.52 ppt·s^{-1} within 100 m above ground in the paint areas of 4000 km^2; while, the annual SO_2 concentration in 2018 was about 6 μg·m^{-3}. Thus, the accumulation coefficient for SO_2 in Beijing was 1382 s on annual average. This accumulation coefficient was in the same order with our estimates of β_1. It implies the reliability of our regression for the spring and fall months. In addition, the regression preforms better in April than in October. It might be explained by the fact that transport gives bigger contribution in October compared to April, but this regression only includes horizontal dispersion and not considers vertical dispersion.

Based on the regression results, the regional transport showed a predominant position with the contribution of >90% during nighttime and the contribution of >60% during daytime. While, the contributions of local photochemical reactions were rising gradually in morning until reaching the relative maximum of ~35% at noon and afternoon. However, on the daily average, the local photochemistry contributed more PAN in April (23.3%) than in October (13.7%). And **Fig. 7** describes the diurnal pattern of the source apportionment results. Approximately, according to the

accumulation coefficient of ~1000 s, during the daytime of January the local photochemistry contributed to PAN by ~0.22 ppb(v), accounting for only 6.8%; but during the daytime of July, this contribution would reach the peak of ~1.29 ppb(v), accounting for 52.1%.

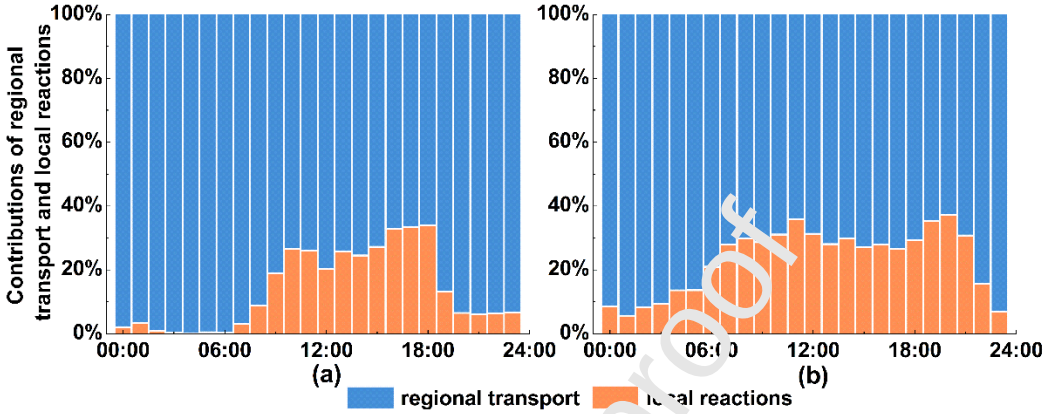

Fig. 7 Average diurnal contributions of local reactions (orange bar) and regional transport (blue bar) to ambient PAN in Oct (a) and Apr (b)

3.5 Photochemical pollution assessment in BTH

PAN at this border site well reflects the influence of transport of PAN among various cities of BTH, especially in non-summer months. So, here we further pay attention to the PAN level with concerned wind directions under different wind speeds, as shown in **Fig. 8**. Considering the apparent influence of solar radiation on PAN during daytime, here we select PAN data in the period of 12:00-16:00 when photochemical pollution is most intense, to explore the transport from various directions and to evaluate the photochemical pollutions in various areas of BTH. In the period 12:00-16:00, under the same wind speed, south winds (including southerly, southwesterly and southeasterly winds) were generally accompanied by the high PAN values in four months. Besides, northeasterly winds in January and northwesterly winds in July also had the higher PAN values. In detail, the higher PAN appeared in the case of south winds at speed of ~2.0 $m \cdot s^{-1}$ for October; in the case of northeastern winds and south winds at speed of 2.5 $m \cdot s^{-1}$, and in the case of small winds at speed of ~0.6 $m \cdot s^{-1}$ for January; in the case of southwesterly and southerly winds at speed of 3~4 $m \cdot s^{-1}$ for April; in the case of northwesterly, southeasterly and southerly winds at

speed of 2~3 $m \cdot s^{-1}$ for July. In three non-summer months, when the wind speed bigger than 2 $m \cdot s^{-1}$, PAN under southerly- or southwesterly- winds was about 0.3 times higher than PAN under southeasterly winds, 1.1 times higher than PAN under northeasterly winds, and 4.9 times higher than PAN under northwesterly winds. All of these illustrate that in non-summer seasons South Hebei and Tianjin had the more severe photochemical pollutions compared to Beijing. However, in July PAN reached 4.19~6.47 ppb(v) under northwesterly winds, 1.02~6.34 ppb(v) under southeasterly winds, and 0.31~6.44 ppb(v) under southerly or southwesterly winds. It implied the photochemical pollutions in the major cities of BTH region was in the equal level in summer. In addition, a weak positive-correlation between PAN and wind speed was also obtained under southwesterly winds during October, January and April, with R of 0.12, 0.07, and 0.20 in respective, which indicated a violent transport of photochemical polluted air masses along southwest-northeast direction in BTH region.

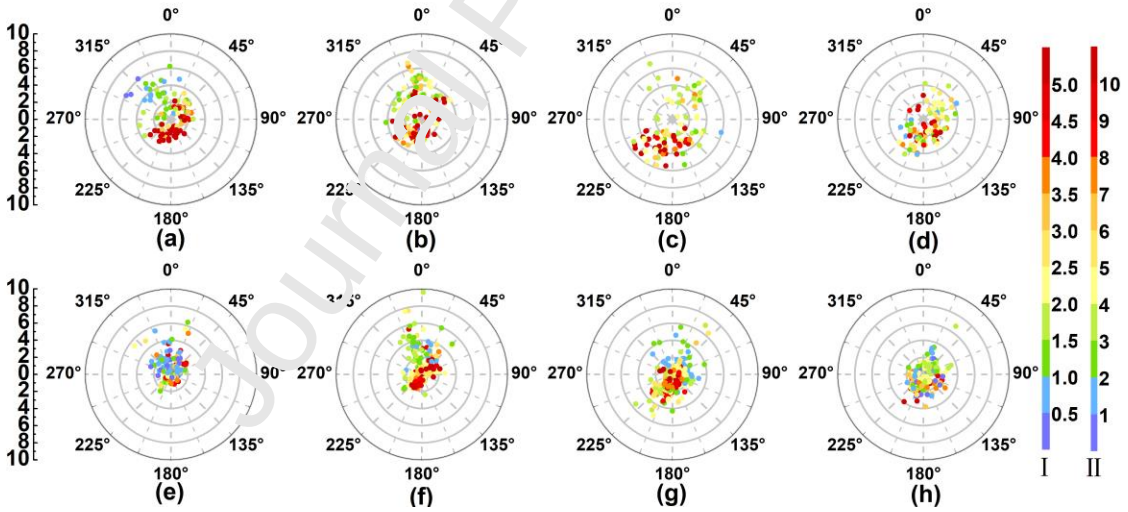

Fig. 8 Scatter plots for PAN concentrations under different wind directions and speeds in 12:00-16:00 of Oct (a), Jan (b), Apr (c), Jul (d) and in the 21:00-05:00 of Oct (e), Jan (f), Apr (g), Jul (h). The legend Ⅰ corresponded to Oct, Jan and Jul, and legend Ⅱ corresponded to Apr.

4 Conclusions

A one-year measurement of atmospheric PAN in the border of Beijing, Tianjin and Hebei in this work revealed a severe photochemical pollution in BTH region, with PAN daily average and daily maximum of 2.23 and 4.67 ppb(v) in October 2018, 3.72

and 6.06 ppb(v) in January 2019, 5.34 and 9.10 ppb(v) in April 2019, 2.44 and 4.95 ppb(v) in July 2019. PAN displayed a unimodal diurnal pattern with the peak values appearing during 14:00-16:00 in three non-summer months, and the dual-peak diurnal pattern was observed with two peaks respectively in 12:00-13:00 and in 20:00-21:00 in July. Strong positive correlation of PAN with CO and with NO_2 in January intimated the important role of tropospheric dispersion in PAN level in winter; while, the weak correlation of PAN with them in October, April and July implied the importance of photochemical pollutions in non-winter seasons. Moreover, $\Delta O_3/\Delta PAN$ analysis implies that the more aged photochemical pollution there in October than in April, and in this border than in urban Beijing.

Furthermore, the PAN yield rate was studied through calculating the photochemical formation and the thermal decomposition of PAN for four months, through estimating PA according to the balance between PAN variation and PAN yield rate during the atmospheric steady days. On daily average, PAN photochemical formation rate was calculated to be 0.48 ppt·s^{-1} (October), 0.091 ppt·s^{-1} (January), 0.96 ppt·s^{-1} (April) and 1.88 ppt·s^{-1} (July); PAN thermal decomposition rate was 0.28 ppt·s^{-1} (October), 0.030 ppt·s^{-1} (January), 0.49 ppt·s^{-1} (April) and 1.80 ppt·s^{-1} (July). Thus, the higher PAN yield rates happened in April (0.47 ppt·s^{-1}) and October (0.20 ppt·s^{-1}) rather than in July (0.08 ppt·s^{-1}) and January (0.07 ppt·s^{-1}).

PSCF analysis showed that the grids that most potentially contribute to high PAN in the border appeared around the site in July, 50~100 km away in direction of southwest in January, but both around this site and along the southwestern trajectory clusters in October and April. The short-range transport of PAN from South Hebei and Tianjin to Beijing was apparently observed in non-summer seasons. Moreover, regression model was developed between PAN and two variables of PAN yield rate and wind speed, to quantify the contributions of regional transport and photochemical formation to PAN. The good regression performance was obtained only for October and April, in which regional transport contributed ~65% PAN at noon time and 77~86% PAN on the daily average. According to the accumulation coefficient (ppb per ppt·s^{-1}), the biggest contribution of photochemical formation to PAN at noon time would reach ~7% in

January and ~52% in July. Therefore, this border site mostly reflects the transport influence among various cities in BTH region. Based on PAN under various winds, it can be seen a more severe photochemical pollution in South Hebei and Tianjin compared to Beijing in non-summer seasons, but a relatively equal photochemical pollution among Beijing, Tianjin and cities of South Hebei in summer.

Acknowledgements

This research was funded by National Natural Science Foundation of China (NSFC) under Grants No. 51678007 and No. 51978010, and Beijing Science and Technology No. Z181100005418015.

References

Beine, H.J., Krognes, T., 2000. The seasonal cycle of peroxyacetyl nitrate (PAN) in the European Arctic. Atmos. Environ. 34, 933–940. doi:10.1016/S1352-2310(99)00288-5

Bridier, I., Caralp, F., Loirat, H., Lesclaux, R., Veyret, B., Becker, K.H., Reimer, A., Zabel, F., 1991. Kinetic and theoretical studies of the reactions acetylperoxy + nitrogen dioxide + M .dblarw. acetyl peroxynitrate + M between 245 and 393 K and between 30 and 760 torr. J. Phys. Chem. 95, 3594–3600. doi:10.1021/j100162a031

Bytnerowicz, A., Fenn, M.E., 1996. Nitrogen deposition in california forests: a review. Science (80-.). 92, 127–146.

Chen, S.X., Liu, H.J., Ye, F.S., Sun, H.X., Guo, B., Liu R., Xiao, J., He J., Zheng X.Y., Wang, H.F., 2019. Air quality assessment report Ⅵ: 2013-2018 regional pollution assessment of 2+43 cities. PKU Stat. Center. http://www.stat-center.pku.edu.cn/docs/20190410102039038516.pdf (in Chinese)

Cooper, O.R., Parrish, D.D., Ziemke, J., Balashov, N. V., Cupeiro, M., Galbally, I.E., Gilge, S., Horowitz, L., Jensen, N.R., Lamarque, J.F., Naik, V., Oltmans, S.J., Schwab, J., Shindell, D.T., Thompson, A.M., Thouret, V., Wang, Y., Zbinden, R.M., 2014. Global distribution and trends of tropospheric ozone: An observation-based review. Elementa 2, 1–28. doi:10.12952/journal.elementa.000029

Dufour, G., Eremenko, M., Beekmann, M., Cuesta, J., Foret, G., Fortems-Cheiney, A., Lachâtre, M., Lin, W., Liu, Y., Xu, X., Zhang, Y., 2018. Lower tropospheric ozone over the North China Plain: Variability and trends revealed by IASI satellite observations for 2008-2016. Atmos. Chem. Phys. 18, 16439–16459. doi:10.5194/acp-18-16439-2018

Fischer, E. V., Jacob, D.J., Yantosca, R.M., Sulprizio, M.P., Millet, D.B., Mao, J., Paulot, F., Singh, H.B., Roiger, A., Ries, L., Talbot, R.W., Dzepina, K., Pandey Deolal, S., 2014. Atmospheric peroxyacetyl nitrate (PAN): A global budget and source attribution. Atmos. Chem. Phys. 14, 2679–2698. doi:10.5194/acp-14-2679-2014

Fischer, E. V., Jaffe, D.A., Reidmiller, D.R., Jaeglé, L., 2010. Meteorological controls on observed peroxyacetyl nitrate at Mount Bachelor during the spring of 2008. J. Geophys. Res. Atmos. 115, 1–18. doi:10.1029/2009JD012776

Gao, T., Han, L., Wang, B., Yang, G., Xu, Z., Zeng, L., Zhang, J., 2014. Peroxyacetyl nitrate observed in Beijing in August from 2005 to 2009. J. Environ. Sci. (China) 26, 2007–2017. doi:10.1016/j.jes.2014.08.002

Hudman, R.C., Jacob, D.J., Cooper, O.R., Evans, M.J., Heald, C.L., Park, R.J., Fehsenfeld, F., Flocke, F., Holloway, J., Hübler, G., Kita, K., Koike, M., Kondo, Y., Neuman, A., Nowak, J., Oltmans, S., Parrish, D., Roberts, J.M., Ryerson, T., 2004. Ozone production in transpacific Asian pollution plumes and implications for ozone air quality in California. J. Geophys. Res. D Atmos. 109, 1–14. doi:10.1029/2004JD004974

Lafranchi, B.W., Wolfe, G.M., Thornton, J.A., Browne, E.C., Min, K.E., Wooldridge, P.J., McKay, M., Goldstein, A.H., Gilman, J.B., Welsh-Bon, D., Kuster, W.C., Degouw, J.A., Mao, J., Chen, Z., Ren, X., Brune, W.H., Cohen, R.C., 2009. Closing the peroxy acetyl (PA) radical budget: Observations of acyl peroxy nitrates (PAN, PPN and MPAN) during BEARPEX 2009. ACS Natl. Meet. B. Abstr. 7623–7641.

Lee, J.B., Yoon, J.S., Jung, K., Eom, S.W., Chae, Y.Z., Cho, S.J., Kim, S. Do, Sohn, J.R., Kim, K.H., 2013. Peroxyacetyl nitrate (PAN) in the urban atmosphere. Chemosphere 93, 1796–1803. doi:10.1016/j.chemosphere.2013.06.019

Li, K., Jacob, D.J., Liao, H., Shen, L., Zhang, Q., Bates, K.H., 2019. Anthropogenic drivers of 2013–2017 trends in summer surface ozone in China. Proc. Natl. Acad. Sci. 116, 422–427. doi:10.1073/pnas.1812168116

Liu, L., Wang, X., Chen, J., Xue, L., Wang, W., Wen, L., Li, D., Chen, T., 2018. Understanding unusually high levels of peroxyacetyl nitrate (PAN) in winter in Urban Jinan, China. J. Environ. Sci. (China). doi:10.1016/j.jes.2018.05.015

Ma, J., Chu, B., Liu, J., Liu, Y., Zhang, H., He, H., 2018. NOx promotion of SO2 conversion to sulfate: An important mechanism for the occurrence of heavy haze during winter in Beijing. Environ. Pollut. 233, 662–669. doi:10.1016/j.envpol.2017.10.103

Malley, C.S., Cape, J.N., Jones, M.R., Leeson, S.R., Coyle, M., Braban, C.F., Heal, M.R., Twigg, M.M., 2016. Regional and hemispheric influences on measured spring peroxyacetyl nitrate (PAN) mixing ratios at the Auchencorth UK EMEP supersite. Atmos. Res. 174–175, 135–141. doi:10.1016/j.atmosres.2016.02.013

McFadyen, G.G., Cape, J.N., 2005. Peroxyacetyl nitrate in eastern Scotland. Sci. Total Environ. 337, 213–222. doi:10.1016/j.scitotenv.2004.06.016

Pandey Deolal, S., Henne, S., Ries, L., Gilge, S., Weers, U., Steinbacher, M., Staehelin, J., Peter, T., 2014. Analysis of elevated springtime levels of peroxyacetyl nitrate (PAN) at the high Alpine research sites Jungfraujoch and Zugspitze. Atmos. Chem. Phys. 14, 12553–12571. doi:10.5194/acp-14-12553-2014

Polissar, A. V., Hopke, P.K., Paatero, P., Kaufmann, Y.J., Hall, D.K., Bodhaine, B.A., Dutton, E.G., Harris, J.M., 1999. The aerosol at Barrow, Alaska: Long-term trends and source locations. Atmos. Environ. 33, 2441–2458. doi:10.1016/S1352-2310(98)00423-3

Qiu, Y., Ma, Z., Li, K., 2019. A modeling study of the peroxyacetyl nitrate (PAN) during a wintertime haze event in Beijing, China. Sci. Total Environ. 650, 1944–1953. doi:10.1016/j.scitotenv.2018.09.253

Russell, A.G., Mcrae, G.J., Cassx, G.R., 1985. The dynamics of nitric acid production and the fate of nitrogen oxides. Atmos. Environ. 19, 893–903.

Singh, H.B., Salas, L.J., 1983. Peroxyacetyl nitrate in the free troposphere. Nature 302, 326–328.

So, K.L., Wang, T., 2003. On the local and regional influence on ground-level ozone concentrations in Hong Kong. Environ. Pollut. 123, 307–317. doi:10.1016/S0269-7491(02)00370-6

Tuazon, E.C., Carter, W.P.L., Atkinson, R., 1991. Thermal decomposition of peroxyacetyl nitrate and reactions of acetyl peroxy radicals with nitric oxide and nitrogen dioxide over the temperature range 283-313 K. J. Phys. Chem. 95, 2434–2437. doi:10.1021/j100159a059

Wang, B.G., Zhu, D., Zou, Y., Wang, H., Zhou, L., Ouyang, X., Shao, H.F., Deng, X.J., 2015. Source analysis of peroxyacetyl nitrate (PAN) in Guangzhou, China: A yearlong observation study, Atmos. Chem. Phys. Discuss. 15, 17093-17133. doi:10.5194/acpd-15-17093-2015

Wang, Y.Q., Zhang, X.Y., Draxler, R.R., 2009. TrajStat: GIS-based software that uses various trajectory statistical analysis methods to identify potential sources from long-term air pollution measurement data. Environ. Model. Softw. 24, 938–939. doi:10.1016/j.envsoft.2009.01.004

Xue, L., Wang, T., Wang, X., Blake, D.R., Gao, J., Nie, W., Gao, R., Gao, X., Xu, Z., Ding, A., Huang, Y., Lee, S., Chen, Y., Wang, S., Chai, F., Zhang, Q., Wang, W., 2014. On the use of an explicit chemical mechanism to dissect peroxy acetyl nitrate formation. Environ. Pollut. 195, 39–47. doi:10.1016/j.envpol.2014.08.005

Zeng, L., Fan, G.J., Lyu, X., Guo, H., Wang, J.L., Yao, D., 2019. Atmospheric fate of peroxyacetyl nitrate in suburban Hong Kong and its impact on local ozone pollution. Environ. Pollut. 252, 1910–1919. doi:10.1016/j.envpol.2019.06.004

Zhang, B., Zhao, X., Zhang, J., 2019. Characteristics of peroxyacetyl nitrate pollution during a 2015 winter haze episode in Beijing. Environ. Pollut. 244, 379–387. doi:10.1016/j.envpol.2018.10.078

Zhang, G., Mu, Y., Zhou, L., Zhang, C., Zhang, Y., Liu, J., Fang, S., Yao, B., 2015. Summertime distributions of peroxyacetyl nitrate (PAN) and peroxypropionyl nitrate (PPN) in Beijing: Understanding the sources and major sink of PAN. Atmos. Environ. 103, 289–296. doi:10.1016/j.atmosenv.2014.12.035

Zhang, G., Mu, Y., Liu, J., Zhang, C., Zhang, Yuanyuan, Zhang, Yujie, Zhang, H., 2014a. Seasonal and diurnal variations of atmospheric peroxyacetyl nitrate, peroxypropionyl nitrate, and carbon tetrachloride in Beijing. J. Environ. Sci. (China) 26, 65–74. doi:10.1016/S1001-0742(13)60382-4

Zhang, H., Xu, X., Lin, W., Wang, Y., 2014b. Wintertime peroxyacetyl nitrate (PAN) in the megacity Beijing: Role of photochemical and meteorological processes. J. Environ. Sci. (China) 26, 83–96. doi:10.1016/S1001-0742(13)60384-8

Zhang, J.B., Xu, Z., Yang, G., Wang, B., 2011. Peroxyacetyl nitrate (PAN) and peroxypropionyl nitrate (PPN) in urban and suburban atmospheres of Beijing, China. Atmos. Chem. Phys. Discuss. 11, 8173–8206. doi:10.5194/acpd-11-8173-2011

Zhang, W.T., Zhang, X.Y., Liu, L., Zhao, L.M., Lu, X.H., 2018. Spatial variations in NO_2 trend in North China Plain based on multi-source satellite remote sensing. J. Remote. Sens. (China) 22,

335 – 346. doi:10.11834/jrs.20187305

Declaration of interests

☒ The authors declare that they have no known competing financial interests or personal relationships that could have appeared to influence the work reported in this paper.

☐The authors declare the following financial interests/personal relationships which may be considered as potential competing interests:

- PAN characteristics at a joint site of BTH were captured during 2018 to 2019.
- We estimated PAN yield rates concerning local photochemistry in different seasons.
- Local photochemistry contributed 52.1% PAN in July at noontime.
- Short-range transport contributed most PAN in non-summer seasons.
- Photochemical pollutions in various cities of BTH were equal in July.
- HB and TJ had more severe photochemical pollutions than BJ in non-summer months.